





## Article

# Discovery of N-Aryl-Benzimidazolone Analogs as Novel Potential HSP90 Inhibitors: A Computational Approach

Radhia Mazri <sup>1</sup>, Lotfi Bourougaa <sup>1</sup>, Afaf Zekri <sup>1</sup>, Mebarka Ouassaf <sup>1,\*</sup> and Bader Y. Alhatlani <sup>2,\*</sup>

<sup>1</sup> Group of Computational and Medicinal Chemistry, LMCE Laboratory, University of Biskra, BP 145, Biskra 07000, Algeria; radhia.mazri@univ-biskra.dz (R.M.); lotfi.bourougaa@univ-biskra.dz (L.B.); afaf.zekri@univ-biskra.dz (A.Z.)

<sup>2</sup> Unit of Scientific Research, Applied College, Qassim University, Buraydah 52571, Saudi Arabia

\* Correspondence: nouassaf@univ-biskra.dz (M.O.); balhatlani@qu.edu.sa (B.Y.A.)

**Abstract:** This study aims to identify *N*-aryl-benzimidazolone analogs as potential inhibitors of the HSP90 protein, which is involved in various diseases. For this, we used computational techniques such as pharmacophoric modeling, virtual screening, in silico ADMET prediction, and molecular dynamics simulations. A target-based pharmacophore model (ADRR) was developed from the MEY ligand to identify the main binding features. This model was used to screen approximately 30,994 similar compounds, leading to the identification of 3019 candidates. Among these, five compounds (L1, L2, L3, L4, and L5) showed strong binding affinity, with docking scores lower than the reference ligand MEY (−7.94 kcal/mol). The ADMET properties of these compounds were favorable, confirming their potential as drug candidates. The two top-performing compounds in the docking studies demonstrated high stability in dynamics studies, the results demonstrated remarkable stability of the ligand–protein complexes, as evidenced by favorable values of metrics such as RMSD, RMSF, Rg, and SASA. These findings provide a promising foundation for further experimental validation and the potential development of effective HSP90 inhibitors.

**Keywords:** HSP90; pharmacophore; virtual screening; ADMET prediction; molecular dynamics simulations



**Citation:** Mazri, R.; Bourougaa, L.; Zekri, A.; Ouassaf, M.; Alhatlani, B.Y. Discovery of N-Aryl-Benzimidazolone Analogs as Novel Potential HSP90 Inhibitors: A Computational Approach. *Appl. Sci.* **2024**, *14*, 10817. <https://doi.org/10.3390/app142310817>

Academic Editors: Stoyanka Atanasova and Vera Gledacheva

Received: 30 October 2024  
Revised: 13 November 2024  
Accepted: 18 November 2024  
Published: 22 November 2024



**Copyright:** © 2024 by the authors. Licensee MDPI, Basel, Switzerland. This article is an open access article distributed under the terms and conditions of the Creative Commons Attribution (CC BY) license (<https://creativecommons.org/licenses/by/4.0/>).

## 1. Introduction

One of the key challenges facing world health today is cancer. An estimated 20 million new instances of cancer were detected globally in 2022, resulting in about 9.7 million deaths. In spite of advances in medical research and treatment, the number of people affected by cancer is still rising. One in five people will have cancer at some point in their lives, and one in nine men and one in twelve women will die from the disease. These alarming figures demonstrate the urgent need for more research and the development of effective medications to treat this pervasive condition [1]. Faced with the alarming increase in cancer cases worldwide, the search for new therapeutic targets, such as HSP90, is becoming crucial to develop more effective treatments. HSP90 (Heat Shock Protein 90) is a chaperone protein essential for the survival of cancer cells, as it stabilizes key proteins involved in tumor growth [2]. Targeting HSP90 with inhibitors disrupts these mechanisms, leading to the degradation of oncoproteins and the death of cancer cells. This therapeutic approach shows promising potential, particularly for cancers resistant to conventional treatments [3].

Recent discoveries regarding HSP90, particularly its isoforms HSP90 $\alpha$  and HSP90B1, have significant implications for cancer treatment, strengthening therapeutic strategies and potentially improving patient outcomes. These findings highlight the crucial role of HSP90 as a key regulator of cancer cell survival and proliferation. HSP90 $\alpha$ , often overexpressed in various cancers, promotes cell growth and resistance to therapies by regulating cell death pathways [4]. Furthermore, HSP90B1 has been identified as a novel biomarker associated with poor prognosis in several cancer types, making it a potential therapeutic target [5].

HSP90 inhibitors, including dual-targeted ones, have shown promising results in preclinical studies, enhancing antitumor effects when combined with other treatments [6]. These inhibitors disrupt oncogenic pathways, leading to the degradation of proteins essential for tumor survival. However, despite this potential, challenges such as drug resistance and toxicity remain major obstacles to their clinical application. Thus, further research is essential to optimize these therapies and improve patient outcomes [4]. The benzimidazole scaffold, a versatile heterocyclic structure, plays a vital role in developing compounds with significant biological and pharmacological properties. First synthesized by Hobrecker in 1872 as 2,5- and 2,6-dimethylbenzimidazole [7], this structure gained prominence after the discovery of N-ribosyl-dimethylbenzimidazole, which acts as cobalt's axial ligand in vitamin B12 [8]. Over time, benzimidazole derivatives have shown immense value in medicinal chemistry, exhibiting a wide range of activities, including antiparasitic (e.g., *albendazole*), antiulcer (e.g., *omeprazole*), antihypertensive (e.g., *candesartan*), antihistaminic (e.g., *bilastine*), anticancer (e.g., *bendamustine*), and antipsychotic effects [9,10].

Chemically, *N*-aryl-benzimidazolones are classified as benzimidazole derivatives with an aryl group attached to the nitrogen atom in the imidazole ring. This structural modification distinguishes these compounds within the broader benzimidazole family, imparting specific physical and chemical properties that enhance biological interactions, particularly for HSP90 inhibition. The *N*-aryl-benzimidazolone class includes compounds known for their ability to inhibit the HSP90 protein [11,12]. However, despite their promising efficacy, some compounds in this family face challenges in terms of metabolic stability, selectivity, and potential toxicity [5,13]. To address these issues, our study employs computational approaches to identify structural analogs that are predicted to retain the inhibitory potential of *N*-aryl-benzimidazolone compounds, with improved pharmacokinetic and safety profiles. Although experimental validation is still needed, this approach provides insights that may aid in discovering optimized HSP90 inhibitors as safer alternatives to current options.

Modeling methods, such as virtual screening, pharmacophore modeling, molecular dock, and molecular dynamics, are crucial tools in the discovery of new drug candidates. Virtual screening often begins with similarity searching, where structural analogs are identified for their potential to share biological activities with a lead compound [14]. Pharmacophore modeling then helps identify chemical features essential for interaction with a target, facilitating the virtual screening of large databases. Molecular docking allows the prediction of the binding affinity between a molecule and a biological target, facilitating the identification of potentially active compounds [15]. Finally, molecular dynamics plays a critical role in assessing the stability and flexibility of molecular complexes [16]. By simulating the motions of molecules over extended periods of time, it provides a deeper understanding of ligand–target interactions, improving the accuracy of predictions regarding compound behavior under realistic biological conditions. These integrated approaches not only reduce development costs and time, but also optimize the targeting of complex pathologies, making the drug discovery process more efficient and accurate.

In light of the modeling methods discussed, we will apply these approaches to explore potential new drug candidates. We will start with a known HSP90 inhibitor and then search for similar compounds in available databases. This similarity search will be followed by pharmacophore modeling to refine the chemical features essential for interaction with HSP90. Then, we will perform molecular docking to assess the binding affinity of the identified compounds with the biological target. Finally, we will use molecular dynamics to verify the stability and flexibility of the proposed molecular complexes. This integrated approach will allow us to efficiently screen compounds and propose potential candidates as new HSP90 inhibitors. Thus, this methodical approach aims to optimize the discovery of new treatments targeting HSP90 and contribute to the advancement of cancer therapies.

## 2. Materials and Methods

### 2.1. Protein and Ligand Preparation

In this study, the HSP90 inhibitor MEY (N-[[1-(5-chloro-2,4-dihydroxyphenyl)-2-oxo-2,3-dihydro-1H-benzimidazol-5-yl]methyl]naphthalene-1-sulfonamide), crystallized with the HSP90 protein (PDB code: 3OWD), was utilized as a reference structure for identifying structurally related compounds. A detailed search of the PubChem database was conducted by using the MEY structure as the query. This was achieved by inputting its SMILES notation and performing a similarity search to retrieve compounds with similar chemical scaffolds. The search results yielded 30,994 compounds that shared structural features with MEY, with a minimum similarity of 80%. These compounds were then filtered using Lipinski's rule of five to assess their drug-likeness and pharmacokinetic properties. The filtering criteria included the molecular weight (less than 500 Da), the octanol–water partition coefficient (LogP less than 5), hydrogen bond donors and acceptors, and the number of rotatable bonds. Compounds that did not meet these criteria were excluded from further analysis, ensuring the selection of drug-like candidates for subsequent molecular docking and dynamics simulations.

The crystal structure of the human HSP90 protein (PDB code: 3OWD, resolution 1.63 Å), obtained from the Protein Data Bank [17], was also used in this study for both protein and ligand preparation. LigPrep (Schrödinger, 2018) was employed to prepare the ligands by optimizing their geometry and protonation states, ensuring their suitability for further computational analysis. Additional methodological details can be found in previous publications from our research group [18].

### 2.2. Molecular Docking

The grid file required for docking was created using Glide's grid-generating panel. The location of the cocrystallized ligand in the protein active site served as the basis for defining the grid's center. Using BIOVIA Discovery Studio Visualizer (Dassault Systems, San Diego, CA, USA), the poses of the ligands with the most advantageous binding energies were displayed following the docking calculations in SP and XP modes.

### 2.3. Pharmacophore Modeling and Virtual Screening

In this research, a pharmacophore model was designed using the "Generate a pharmacophore from a protein–ligand complex" function in the Phase module, while maintaining the default parameters. This model was then used to perform a virtual screen on a database of similar compounds from PubChem. Following this screening, 3019 compounds from the PubChem database were identified and selected based on their correspondence with the criteria defined by the pharmacophoric model.

### 2.4. ADME-T and Drug-Likeness Properties

When a drug is supplied to a human, it must have appropriate properties for ADME. Given this, determining the safety or toxicity profiles for any drug candidate by *in silico* ADMET analysis is an important stage in the drug development process [19]. The ADMETlab 2.0 server (obtained on 24 February 2024) [20] was used to predict the ADMET profile of the top lead compounds. In addition, the ProTox-II web server [21] was utilized to test the compounds' cytotoxicity, mutagenicity, immunotoxicity, carcinogenicity, and hepatotoxicity.

### 2.5. Molecular Dynamics Simulation

According to the results of the molecular docking analysis and ADMET evaluations, three different complexes were submitted to all-atom molecular dynamics simulations: HSP90\_L1, HSP90\_L2, and HSP90\_MEY as a reference complex. The three simulations were run at 300 ns with the CHARMM36 force field from the Gromacs-2023 program. The molecular topology data of the identified inhibitors and the reference drug (MEY) were derived from the SwissParam platform (<http://swissparam.ch/> accessed on 10 June

2024) [22]. Additionally, the editconf function was used to create a simulation box on the complex with an absolute minimum distance of 10 Å to any wall. Furthermore, the intermolecular potential using the TIP3P water model was utilized to fill the box with solvent molecules with the application of the *gmx* solvate command [22]. The charge for each system was neutralized by the addition of (Na<sup>+</sup>, Cl<sup>-</sup>) ions. The steepest descent technique (1000 ps) for protein configuration was used to minimize the energy. For energy minimization, set nsteps to 50,000 were modified to an energy step size (emstep) of 0.01 [23]. NVT equilibration was conducted at 300 K for 500 ps using a V-rescale thermostat. The NPT was then adjusted for 100 ps using a Berenson pressure-coupling system and a coupling value of 2.0 ps. Finally, the MD simulation was performed at 300 ns for each system, using nsteps of 150,000,000 specified in the md.mdp data.

We analyzed the MD simulation results to gain understanding of the compactness, flexibility, and stability of the complexes that were produced. While the root mean square fluctuation (RMSF) was used to evaluate the flexibility of all residues, the root mean square deviation (RMSD) was used to determine the structural change of each system during 300 ns of simulation. Each complex's compactness was ascertained using the radius of gyration (Rg). In order to assess the overall stability of the complexes that were generated, we also calculated the solvent-accessible surface area (SASA). To analyze the simulated trajectories, the Grace program (<http://plasma-gate.weizmann.ac.il/Grace/> accessed on 12 June 2024) was used. Lastly, we used the free energy landscape (FEL) to investigate the systems' molecular stability.

### Calculating Binding Free Energy

The molecular mechanics Poisson–Boltzmann surface area (MM-PBSA) is a popular approach for estimating a protein–ligand complex's binding free energy. The MM-PBSA binding free energy ( $\Delta G_{\text{bind}}$ ) evaluation was performed using the *g\_mmpbsa* tool's specified technique. The binding free energy was computed in the following way:

$$\Delta G_{\text{bind}} = G_{\text{complex}} - (G_{\text{protein}} + G_{\text{ligand}})$$

Here,  $G_{\text{complex}}$  indicates the native protein's binding energy, whereas  $G_{\text{protein}}$  and  $G_{\text{ligand}}$  reflect the protein's and ligand's binding energies.

## 3. Results

### 3.1. Target-Based Pharmacophore Modeling

We want to find drugs that suppress the human HSP90 protein to treat cancer. We created a target-based pharmacophore model using the Schrödinger software, 2018, suite and the human HSP90 protein structure. The MEY–HSP90 complex from XP docking was used to generate the pharmacophore model. We found the best MEY ligand binding arrangement in the HSP90 protein binding site using XP docking. Figure 1 shows that our pharmacophore model revealed essential properties for successful inhibition by examining ligand–protein interactions.

The ADDRR pharmacophore model has one hydrogen bond acceptor, two donors, and two hydrophobic groups.

Before employing the pharmacophore model in screening, it is essential to validate its ability to accurately distinguish active inhibitors from non-active compounds. In this study, we utilized enrichment-based validation to ensure that the model reliably prioritizes active molecules. We compiled a validation set comprising 35 active compounds identified from the literature [24], along with 1000 decoys obtained from the DUD-E decoy database. This approach allows us to evaluate the model's sensitivity and specificity in identifying potential inhibitors among a large set of decoys. The pharmacophore model validation results (Table S1) demonstrate strong predictive capabilities, underscoring the model's efficiency in distinguishing active HSP90 inhibitors from decoys. The high BEDROC scores across varying alpha values, especially the 0.955 score at the strictest alpha (160.9), suggest

that the model excels at early recognition of actives. This is complemented by the ROC value of 0.83, which confirms the model's accuracy in classifying actives versus decoys. Additionally, the RIE value of 11.39 and an area under the accumulation curve of 0.85 indicate substantial enrichment, meaning that the model prioritizes actives within the ranked list effectively, which is crucial for streamlined screening. Moreover, the distribution data reveal that a significant portion of actives—up to 77.1%—appears within the top 20% of results, further affirming the model's capacity to rank potential inhibitors at the forefront. With 30 out of 35 actives correctly ranked and an average of 33 decoys outranked by each active, these metrics highlight the model's robustness and reliability, suggesting that it can play a valuable role in the efficient identification of promising HSP90 inhibitors for subsequent validation steps. A detailed analysis, including the ROC curve and additional metrics, is provided in the Supplementary Figure S1.

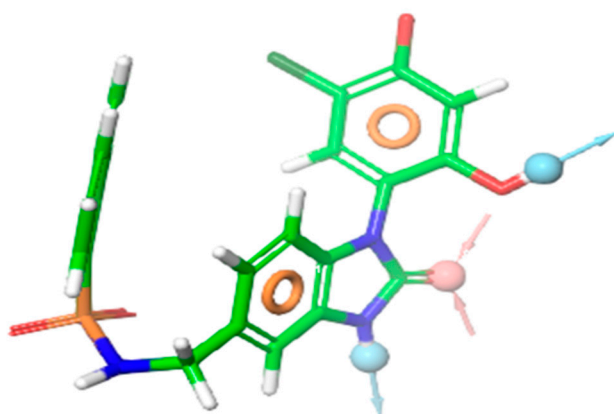


**Figure 1.** Pharmacophore model ADDRR: acceptor (red), donor (blue), and ring (orange) representation.

Our pharmacophore model ADDRR was then used to screen related compounds. We accurately discovered 3019 compounds that closely fitted the model and met its 4–5 feature super-positions throughout screening.

### 3.2. Target-Based Virtual Screening and Molecular Docking

Target-based virtual screening (TBVS) is widely used to identify potential drug candidates by focusing on interactions with specific molecular targets. In our study, we selected compounds that met Lipinski's drug-likeness criteria [17] and aligned with the pharmacophore model designed for targeting the HSP90 protein. These selected compounds were further analyzed through molecular docking experiments to evaluate their interactions and binding affinity with HSP90. The docking results revealed binding patterns, energy scores, and potential interactions between the compounds and the HSP90 protein.

Our research involves redocking the reference ligand MEY to test our molecular docking technique's accuracy and reliability. Figure 2 shows that our enzyme active site determination was accurate RMSD: 1.553. HSP90's binding pocket had two components: a hydrophobic component with Ala55, Ile96, Met98, Leu107, Phe138, and Val150, and a hydrophilic component with Asn51, Asp93, and Thr184. These findings support previous research [25].

To improve the accuracy and efficiency of our screening process, we first employed the standard precision (SP) docking approach, which is fast and allows selecting compounds capable of forming stable complexes. Subsequently, the compounds, identified by SP, were subjected to a more precise docking analysis using the extra precision (XP) approach [26]. The strength of the binding between the chemical compounds and the protein target is shown by the results obtained during the docking process. Lower scores indicate higher binding strength between the chemical and the protein; the interactions in the docking process can be better understood by analyzing and interpreting these results.

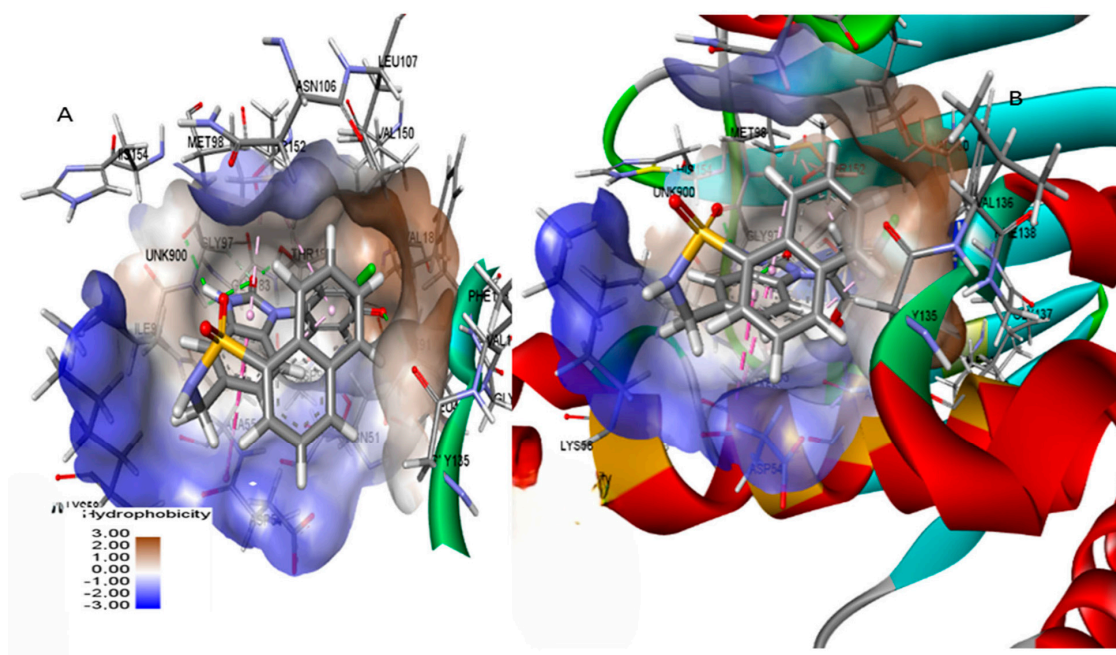


**Figure 2.** (A): Visual representation of the HSP90 protein and the chemical MEY that have been crystallized together. (B): The surface of hydrophobic residues in the cavity is shown.

Five compounds (L1, L2, L3, L4, and L5) displayed docking scores lower than the reference ligand MEY ( $-7.94$  kcal/mol), indicating strong binding affinities (Table 1). This suggests that these compounds bind more effectively and stably to the N-terminal ATP-binding region of HSP90. A visual analysis of the complex interactions, as shown in Figure 3, allowed us to further examine the docking data. For an overview, Table S2 summarizes the types of interactions observed. Hydrogen bonds, which are known for their electrostatic strength and ability to stabilize ligand–receptor complexes, were essential in our compounds' binding to HSP90, specifically involving residues Gly97, Thr184, Asn51, and Asp93 [27–29]. Notably, these same residues were observed in the binding of the reference ligand MEY, indicating a shared interaction pattern and consistent binding mode that support the reliability of our docking results. Both hydrophobic interactions and hydrogen bonding were present between our compounds and HSP90, specifically with residues Met98, Ala55, Asp54, and Phe138, consistent with prior findings [18,22]. Particularly, Met98 forms a pi–sulfur interaction with our compounds; in this noncovalent interaction, the pi-electron system of the aromatic rings aligns with the sulfur atom in methionine, which enhances ligand–protein affinity. Multiple interactions with the protein improve the stability of our compounds within the active site, suggesting their strong potential as HSP90 inhibitors. A summary of the compounds' properties is provided in Table S3. The pharmacokinetics and drug-likeness profiles of these candidates will be discussed in the following section.

**Table 1.** SP and XP docking binding energy in kcal/mol. Method for finding the best chemicals.

Compound	CID	SP (kcal/mol)	XP (kcal/mol)
L1	CID69438556	$-7.910$	$-9.795$
L2	CID69441313	$-9.373$	$-9.636$
L3	CID117208203	$-8.687$	$-8.687$
L4	CID52948538	$-8.383$	$-8.383$
L5	CID117209048	$-8.262$	$-8.264$
MEY	CID 50925477	$-7.225$	$-7.946$

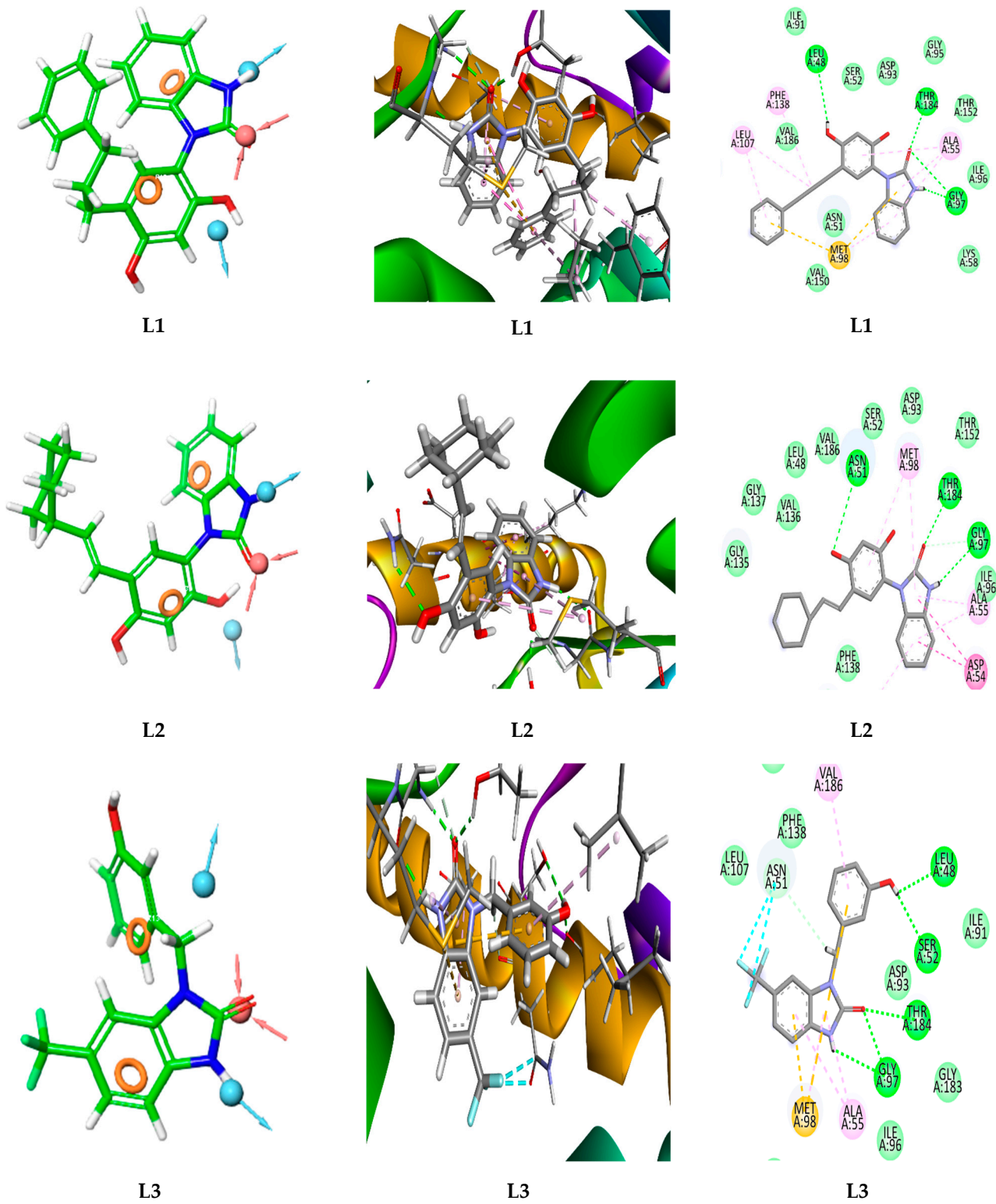
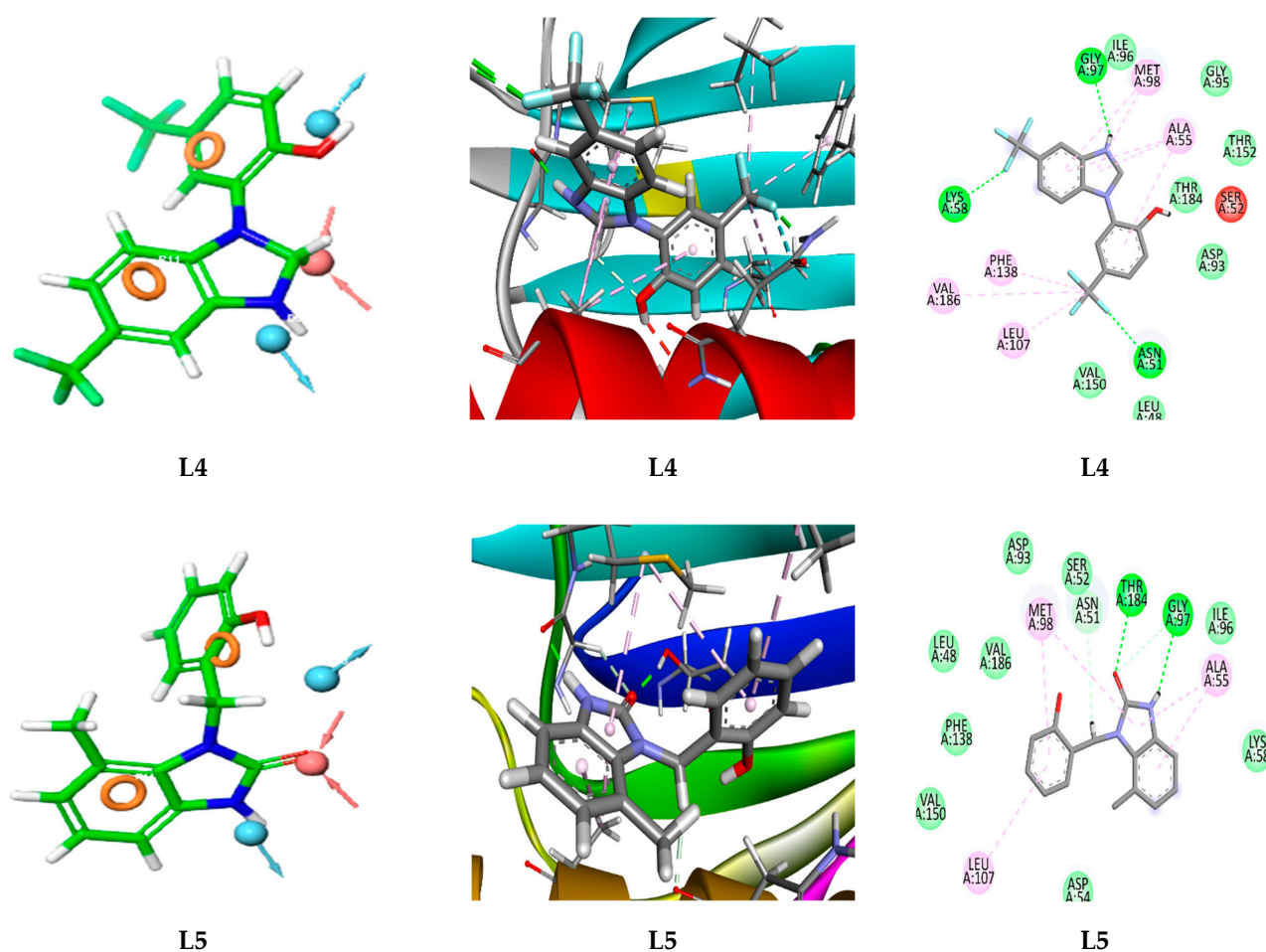


Figure 3. Cont.



**Figure 3.** Highest-ranking compounds were assessed for their adherence to the structure-based pharmacophore model ADDR, as well as their 2D mapping and 3D interactions within the binding area of the HSP90 protein (PDB ID: 3OWD).

### 3.3. ADMET Profiles of the Lead Compound

Pharmacokinetic aspects are important when it comes to evaluating the indemnity and efficacy of a lead compound [30]. In this study, various properties, including physicochemical, medicinal, pharmacokinetics, and toxicity, were examined for the top lead compounds obtained (L1, L2, L3, L4, and L5).

### 3.4. Physicochemical Properties

Table 2 presents the physicochemical properties of the selected compounds, which have a lower molecular weight and volume (<380) compared to the reference ligand MEY, potentially enhancing their therapeutic properties and interactions with HSP90. The lead compounds contain an acceptable number of rings (3–4) and heteroatoms (4–9) within optimal ranges, supporting effective interactions within the protein's active site. Flexibility values range from 0.118 to 0.217, with L1 being the most flexible, aiding in adaptability to the binding site. High bioavailability is confirmed for all compounds through total polar surface area (TPSA) values (35–79 Å<sup>2</sup>) and rotatable bonds (2–5), with L1 and L2 having the highest TPSA values. All compounds have suitable solubility values (Log S) except for L4, which may face membrane permeability issues. The octanol–water partition coefficient (log P) for L4 is ideal (0–3), with other compounds having acceptable values except L2, which slightly exceeds the optimal range. Table 2 highlights a correlation between logD and logP values, with L5 achieving the best logD at 2.963.



**Table 2.** Physicochemical properties of the top lead compounds.

Comp.	L1	L2	L3	L4	L5	MEY
MW	360.150	350.160	308.080	348.070	254.110	495.070
Volume	376.842	364.819	281.648	293.697	263.446	459.902
n-Rot	5	3	3	3	2	5
nRing	4	4	3	3	3	5
nHet	5	5	7	9	4	10
Flexibility	0.217	0.125	0.176	0.188	0.118	0.167
TPSA	78.250	78.250	58.020	35.500	58.020	124.420
logS	−3.958	−3.931	−3.971	−5.746	−3.045	−4.776
logP	4.422	5.019	3.464	4.655	2.836	4.562
logD	3.937	4.146	3.674	4.138	2.963	3.492

### 3.5. Medicinal Chemistry

In drug design, the Lipinski Rule, Pfizer Rule, GSK Rule, and the concept of the Golden Triangle are key guidelines for selecting compounds with high potential for therapeutic efficacy and safety. The Lipinski Rule of Five [31] outlines criteria for oral bioavailability, including limits on the number of hydrogen bond donors and acceptors, a molecular weight under 500 Da, and a LogP value below 5. The Pfizer Rule [32], or “3/75 rule”, focuses on reducing toxicity linked to high lipophilicity (LogP > 3) and low polar surface area (TPSA < 75 Å<sup>2</sup>). The GSK Rule [33] suggests that compounds with a molecular weight over 400 Da and a LogP above 4 may face challenges in pharmacokinetics and safety. Finally, the Golden Triangle [34] concept targets optimal ranges of molecular weight, lipophilicity, and polar surface area, where compounds achieve a balanced profile of efficacy, safety, and bioavailability. Table S4 outlines the medicinal chemistry properties of the lead compounds as predicted by ADMETlab 2.0. Compounds L3, L4, and L5 demonstrate strong drug-likeness with high quantitative estimate of drug-likeness (QED) scores (>0.67). All compounds show favorable synthetic accessibility (SA score < 6), indicating ease of synthesis. L5 meets the criteria of Lipinski, Pfizer, GSK, and Golden Triangle rules, reflecting excellent bioavailability and promising drug-likeness. Compounds L1 and L2 meet all criteria except the GSK Rule due to logP values over 4. Compounds L3 and L4 do not meet the Pfizer Rule, suggesting potential toxicity risks. No compounds raised alerts for PAINS or BMS, indicating a lower risk of false-positive or misleading outcomes.

### 3.6. Absorption and Distribution

Table 3 presents absorption and distribution properties for the compounds. All compounds show favorable Caco-2 permeability (>−5.15) and high passive MDCK permeability, except L4, which has intermediate permeability. Compounds L2, L3, and L5 effectively inhibit plasma glycoprotein (PGP), with L4 showing moderate inhibition. All lead compounds show low human intestinal absorption (HIA < 30%, values < 0.1), indicating potential for poor intestinal absorption. Only L3 and L4 display favorable oral bioavailability at 20%, while other compounds exceed a permeability threshold of 0.7. High plasma protein binding (PPB > 95%) suggests a limited therapeutic index. Volume of distribution (VD) values (0.196–4.954 L/kg) indicate appropriate distribution, but only L3 has moderate blood–brain barrier (BBB) penetration, potentially affecting the CNS, while other compounds show minimal BBB penetration (<0.3).

**Table 3.** In silico prediction of absorption and distribution of the top lead compounds.

Comp.	L1	L2	L3	L4	L5	MEY
Absorption						
Caco-2 Permeability	−5.108	−5.030	−4.849	−4.989	−4.815	−5.856
MDCK Permeability	$1.8 \times 10^{-5}$	$2.3 \times 10^{-5}$	$1.2 \times 10^{-5}$	$9.2 \times 10^{-6}$	$2.7 \times 10^{-5}$	$1.3 \times 10^{-5}$
Pgp-inhibitor	poor	excellent	excellent	medium	excellent	medium
HIA	excellent	excellent	excellent	excellent	excellent	medium
F20%	poor	poor	excellent	excellent	poor	excellent
Distribution						
PPB	97.989%	98.221%	95.037%	98.178%	95.329%	98.622%
VD L/Kg	0.501	0.196	0.781	4.954	0.424	0.429
BBB Penetration	excellent	excellent	medium	excellent	excellent	excellent

<0.3; excellent, 0.3–0.7; medium, 0.7–1.0; poor.

### 3.7. Metabolism and Excretion

The ability of an active substance to inhibit certain enzymes is of crucial importance in the development of new drugs and in clinical applications. To better understand a compound's pharmacokinetic characteristics and maximize its therapeutic application, it is important to determine which enzymes it inhibits. Based on the data in Table S5, all compounds may be potent cytochrome P450 (CYP) inhibitors. All compounds exhibited moderate renal clearance, with values ranging from 6.567 to 11.818. Compound L5 exhibited the highest value. With the exception of compound L4, which had a low value of 0.051, all compounds have an intermediate half-life ( $T_{1/2}$ ), ranging from 0.568 to 0.892. It is important to remember that drugs with short half-lives and poor clearance are generally excreted comparatively quickly [35,36].

### Prediction of Toxicity

The ADMETlab 2.0 server showed that the five lead compounds would not block the human ether ago-ago gene (hERG) (hERG score < 0.3), meaning that these compounds would not cause cardiotoxicity. Furthermore, they would not cause acute oral toxicity in rats, like MEY, which provides visions of possible dangers related to their ingestion. Determining the mutagenic potential of a compound is crucial for drug development, as substances that are too toxic can never be employed as drugs [37]. Table S6 shows that compound L3 has a safety profile in terms of mutagenicity, like MEY, but compounds L4 and L5 were classified as moderately mutagenic, while the remaining compounds were toxic. Only compounds L3, L5, and MEY did not cause skin sensitization; compound L4 has a moderate effect, while compounds L1 and L2 are considered sensitizers. Compounds L2 and L4 showed respiratory toxicity, while compound L3 was moderately harmful. The other compounds did not show any respiratory toxicity (Table S6).

Table S7 summarizes the toxicity predictions obtained with the Protox-II platform. According to the data, the probability that one of the studied compounds is hepatotoxic, carcinogenic, immunotoxic, mutagenic, or cytotoxic is low. On the other hand, MEY is not immunotoxic, mutagenic, carcinogenic, or cytotoxic but could be hepatotoxic with a probability of 0.55.

### 3.8. Molecular Dynamics Simulations

Based on the docking results and confirmation of favorable ADME properties, we selected compounds L1 and L2 for further in-depth analysis through molecular dynamics simulations. We began by calculating the variation in the overall stability of the three systems' backbone atoms using the RMSD (nm) measurements. The root mean square deviation values of the created systems were compared with the reference complex (HSP90\_MEY)

over 300 ns of simulation. Figure 4 depicts the RMSD profile for each investigated system. The RMSD description of the HSP90\_L1 complex was substantially more stable, with an average RMSD of 0.1219 nm, compared to the reference complex (with an average RMSD of 0.413 nm). At the molecular level, compound L1 established a very stable complex with the HSP90 receptor, allowing it to selectively inhibit the protein's essential and biological functions. In addition, the average RMSD value of the HSP90\_L1 complex was 0.288 nm. This measurement demonstrates that compound L2 forms a less stable complex with the active site of HSP90 than compound L1, although it is more stable than the reference drug (MEY). Moreover, The RMSD measures how a protein's backbone changes from its initial to its final structural state. Multiple studies have consistently found RMSD values ranging between 0 and 0.3 nm in their analyses of molecular dynamics simulations. Ultimately, the findings suggest that compounds L1 and L2 can be promising selective drugs in oncology. The average values of the various features acquired over a 300 ns period by molecular dynamics simulation are shown in Table 4. Furthermore, when comparing the reference system to the detected compounds (L1 and L2) during binding, the average RMSF values of all residues were almost the same. Each system's RMSF profile showed variations from its original structures, pointing to minor dynamic alterations, as can be seen in Figure 5. Moreover, all of the systems' variations matched those of the MEY medication, demonstrating the structural stability of the systems being investigated. These suggested chemicals hold promise as possible candidates for the development of targeted and efficient treatments for incurable diseases, given the consistent results of RMSF and RMSD investigations.

**Table 4.** Mean values of various features from 300 ns MD simulations.

System	HSP90_L1	HSP90_L2	HSP90_MEY
RMSD (nm)	0.219	0.288	0.413
RMSF (nm)	0.164	0.175	0.164
Rg (nm)	1.724	1.739	1.707
SASA (nm <sup>2</sup> )	112.311	113.561	111.869

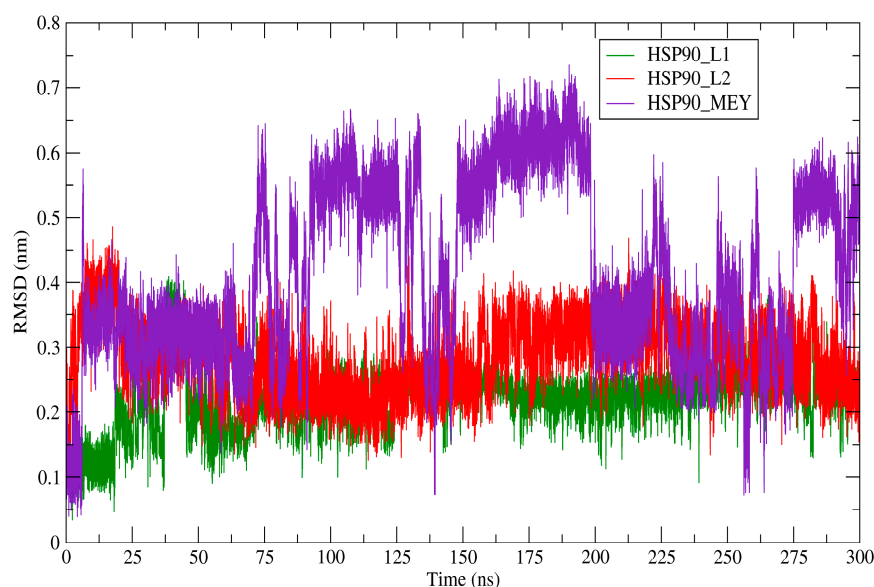


**Figure 4.** Analysis of root mean square deviation for the backbone atoms and complexes of HSP90.

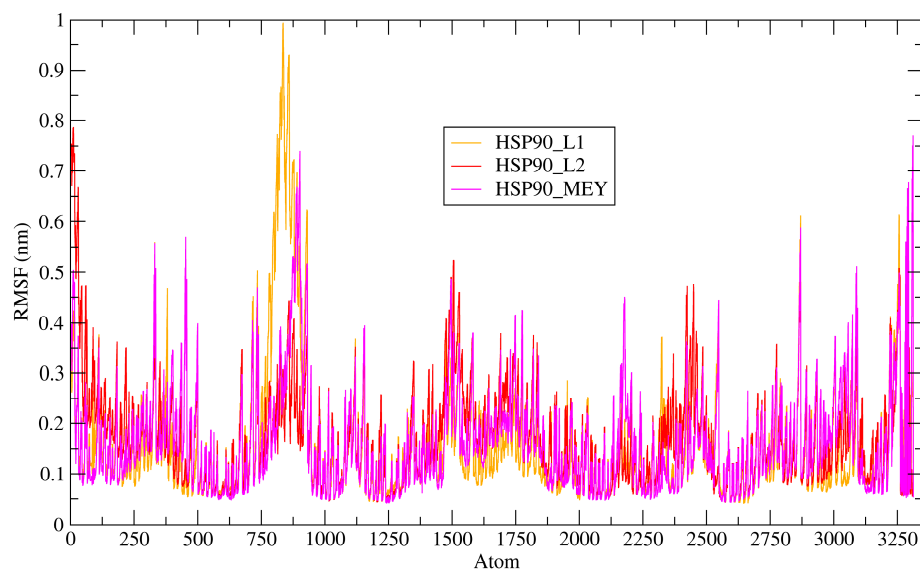


**Figure 5.** Backbone atomic variability in HSP90 and its complexes: RMSF analysis.

HSP90's structural compactness was assessed using  $R_g$ . The results revealed that  $R_g$  values across all complexes exhibited slight variations, ranging from 1.707 to 1.739 nm. The average  $R_g$  values calculated for the HSP90\_L1, HSP90\_L2, and HSP90\_MEY complexes were 1.724 nm, 1.739 nm, and 1.707 nm, respectively. The HSP90 configuration remained unchanged in the presence of the proposed inhibitors, maintaining a stable radius of gyration throughout the 300 ns simulation period, indicating the stability of all complexes. Figure 6 shows the radius of gyration. The solvent-accessible surface area (SASA) predicts the dynamic changes observed during the interaction time. Figure 7 shows SASA profiles for each system during 300 ns of simulation. The average solvent-accessible surface area for the reference system measured  $111.869 \text{ nm}^2$ , while for the complexes HSP90\_L1 and HSP90\_L2, the average SASA values were  $112.311 \text{ nm}^2$  and  $113.561 \text{ nm}^2$ , respectively. The SASA reached a stable equilibrium throughout the simulation, suggesting that the configurations of HSP90 remained stable in the presence of the proposed inhibitors (L1 and L2). This consistency helps elucidate how the proposed molecules interact with the active site of HSP90 and consistently bind during molecular binding.

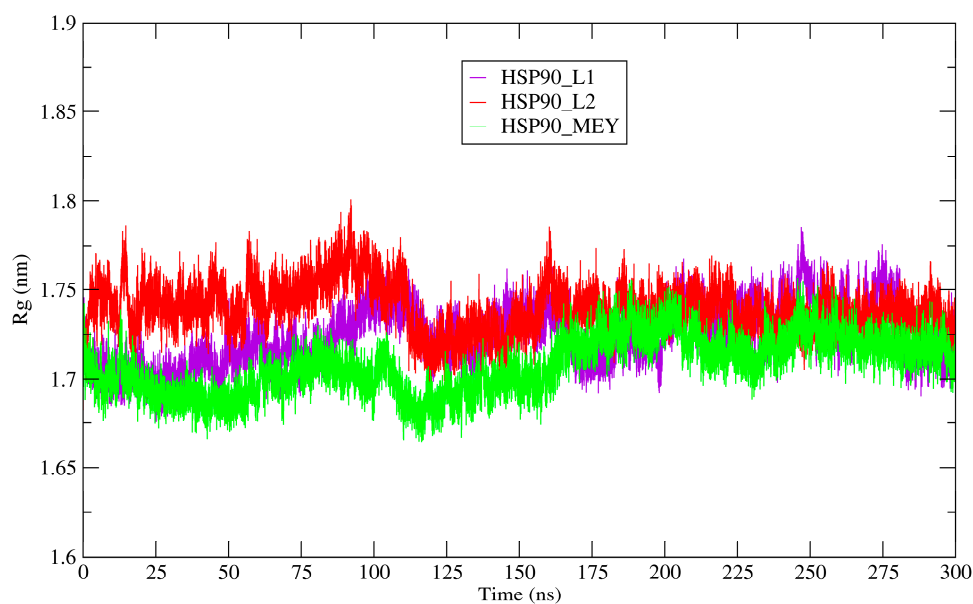


**Figure 6.** Radius of gyration profiles for each complex during 300 ns of simulation.

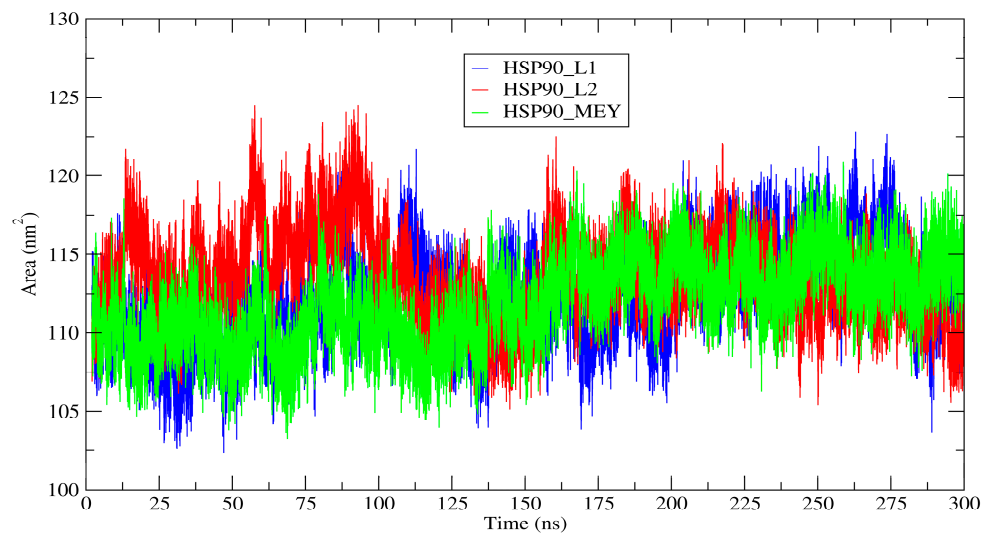


**Figure 7.** SASA profiles for each system over 300 ns of simulation.

These findings align with previous research, specifically the docking study, which demonstrates that the proposed compounds form highly stable complexes with the HSP90 protein and effectively inhibit its crucial function. Moreover, snapshots of the three systems were taken at intervals of 100 to 300 ns. Analysis of the binding poses of each complex confirms their stability throughout the simulation period, as shown in Figure 8.

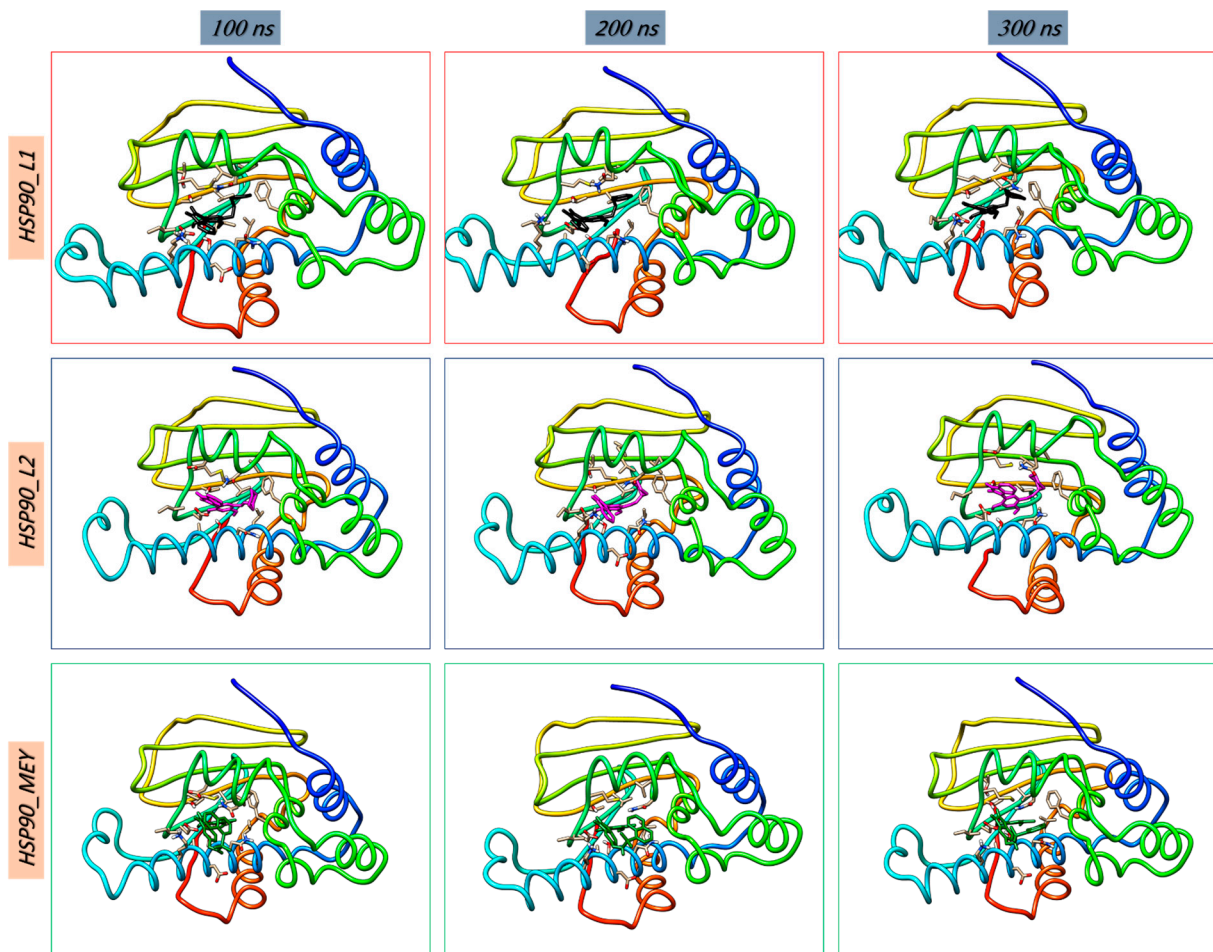


**Figure 8.** Binding poses of the three systems during 300 ns of simulation.

### Free Energy Landscape

The FEL (free energy landscape) technique is instrumental in identifying the representative conformational state of a system. This state is ascertained by pinpointing the minimum on the FEL, which represents the most stable structural minimum or the equilibrated conformational state. To examine the structural shift of the HSP90 protein following the biomolecular interactions in each system, we generated an FEL to illustrate changes in the protein's configuration. We utilized two specific reaction parameters for the FEL analysis: the RMSD of the HSP90 protein, which reflects the protein's structural stability over 300 ns of simulation, and the  $R_g$ , which provides insight into the protein's folding behavior. Figure 9 depicts the FEL right after interactions with HSP90 and the L1, L2, and MEY molecules.

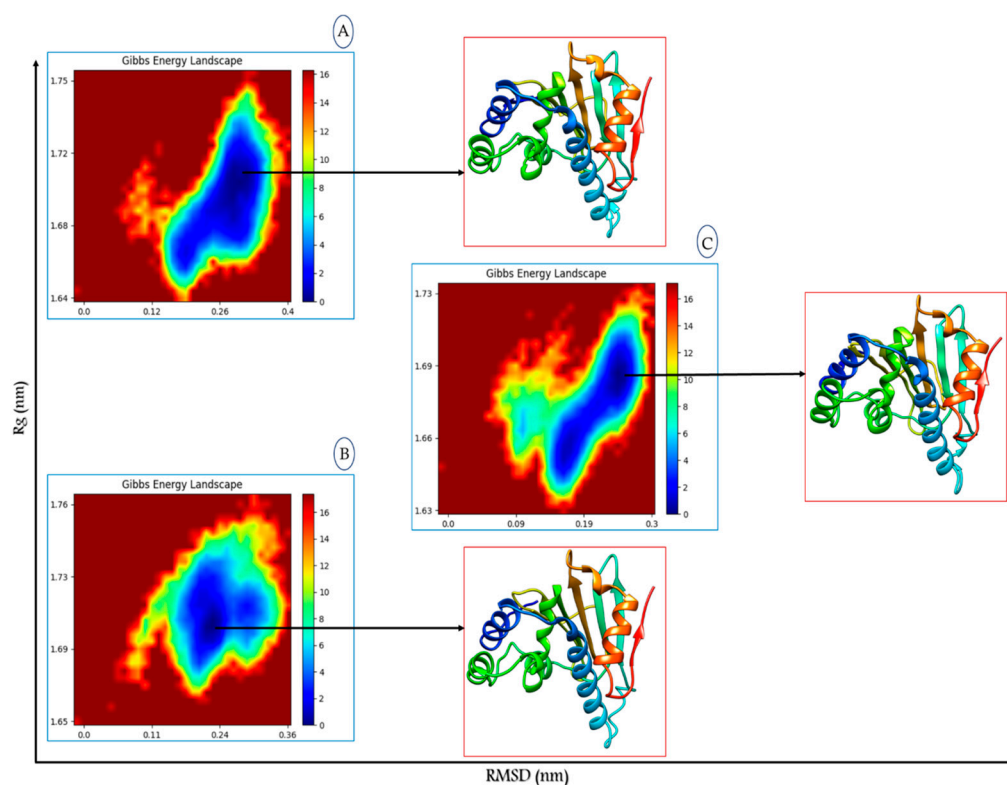


**Figure 9.** Free energy landscape as a function of RMSD and  $R_g$ ; (A) HSP90\_L1, (B) HSP90\_L2, (C) HSP90\_MEY and the extracted HSP90 structures from minimum energy.

First, we identified a prominent well at RMSD values of 0.140 to 0.200 nm and  $R_g$  values of 1.65 to 1.73 nm when HSP90 interacted with the proposed molecule L1. In addition, upon interaction with the second proposed molecule L2, a distinct well was observed, concentrated at  $R_g$  values of 1.67 to 1.74 nm and RMSD values of 0.11 to 0.30 nm. On the other hand, across interactions with the reference medication (MEY), we definitely identified a centered zone at RMSD (0.12, 0.25 nm) and  $R_g$  (1.64, 1.71 nm). The simulations suggest that the low-energy regions on the free energy maps indicate a reasonably stable biomolecular structure and dynamics. Compounds L1 and L2 form highly stable complexes with the protein receptor, unlike the medication MEY, as further corroborated by the conspicuous wells seen in the free energy landscape maps when these molecules are attached to the HSP90 receptor. Finally, the extraction of HSP90 structures from the three regions indicated minimal conformational changes in the HSP90 configurations following interaction with the proposed inhibitors.

### 3.9. Binding Free Energy Calculation

To fully analyze the binding energies connected to the three ligands' interactions with the protein receptor, MM-PBSA calculations were carried out [38]. In many cases, noncovalent interactions are important in molecular interactions. Van der Waals interactions and electrostatic forces are two examples of these interactions, and they can both have a positive or negative effect on the total binding energy. For each system, Table 5 shows the binding free energy expressed in kcal/mol. The binding of the three complexes was characterized by a high frequency of electrostatic interactions, with  $-53.49$ ,  $-41.46$ , and  $-40.74$  kcal/mol for the HSP90\_L1, HSP90\_L2, and HSP90\_MEY complexes, respectively. Furthermore, the suggested inhibitors L1 and L2 formed a stable complex with the HSP90 receptor in comparison to the reference drug MEY. The results of this study demonstrate that these designed inhibitors possess the potential to inhibit the vital activity of the HSP90 protein, and the docking modeling findings have been validated.

**Table 5.** Binding free energy, reported in kcal.mol<sup>-1</sup> for each system, was computed using MM-PBSA techniques.

	HSP90_L1	HSP90_L2	HSP90_MEY
$\Delta E_{VDW}$	$-39.99$	$-35.12$	$-37.74$
$\Delta E_{EEL}$	$-53.49$	$-41.46$	$-40.74$
$\Delta E_{PB}$	$63.30$	$48.18$	$51.44$
$\Delta E_{NPOLAR}$	$-4.14$	$-3.81$	$-3.93$
$\Delta G_{GAS}$	$-93.49$	$-76.58$	$-78.48$
$\Delta G_{SOLV}$	$59.16$	$44.37$	$47.51$
$\Delta_{TOTAL}$	$-34.33$	$-32.21$	$-30.97$

## 4. Discussion

In this study, we aimed to identify *N*-aryl-benzimidazolone analogs as potential inhibitors of the HSP90 protein, a chaperone involved in multiple signaling pathways and associated with diseases like cancer and inflammatory conditions.

In this study, we focused on the design and analysis of *N*-aryl-benzimidazolone derivatives as potential inhibitors of the HSP90 protein, which plays a crucial role in numerous signaling pathways related to cancer, inflammation, and other diseases [39]. Our approach combined pharmacophoric modeling, molecular docking, and molecular dynamics simulations to explore the interactions between these compounds and HSP90, as well as their physicochemical and pharmacokinetic properties.

The pharmacophore model developed from the MEY ligand successfully highlighted key features for effective binding in the HSP90 active site. These features included hydrogen bonding and hydrophobic interactions, which are well-documented in the literature as critical for HSP90 inhibition [40]. The selected compounds demonstrated compatibility with these critical binding characteristics, showing a similar interaction profile to the MEY ligand. Specifically, hydrophobic interactions with residues such as Met98 and Ala55 played an essential role in stabilizing the ligand–protein complex. This supports the notion that these compounds are capable of mimicking known interaction patterns, which is crucial for developing effective inhibitors [41].

The physicochemical properties of the top lead compounds were also favorable for drug development. Their molecular weights and volumes were within acceptable limits, ensuring good pharmacokinetics. The TPSA values indicated adequate membrane permeability, while the LogP values were generally optimal for effective distribution, aligning with the expected range for drug-like molecules. However, some compounds showed slightly lower solubility, which could affect bioavailability; this is consistent with findings from other studies that emphasize the importance of balancing solubility and lipophilicity

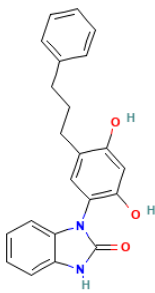
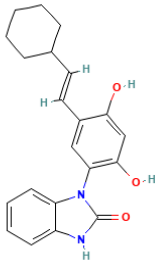
for drug efficacy [42]. Nevertheless, the overall drug-likeness scores derived from ADMET predictions confirmed that these compounds hold promise for further optimization.

Our molecular dynamics simulations revealed that compound L1 exhibited exceptional stability in its complex with HSP90, with an average RMSD of 0.1219 nm, much lower than the reference drug MEY (0.413 nm). This indicates that L1 formed a highly stable complex with the HSP90 protein, which is a critical factor for the selective inhibition of its function. On the other hand, compound L2 showed a slightly less stable interaction but still demonstrated better stability than MEY. These findings align with previous studies, which also reported that lower RMSD values correlate with stronger and more stable ligand–protein binding [43]. Moreover, the RMSF and Rg analyses confirmed that the structural integrity of HSP90 was well-maintained during the simulations, even in the presence of the proposed inhibitors. The consistent SASA profiles further supported the notion that L1 and L2 interact stably with the protein’s active site, facilitating efficient binding throughout the simulation period.

The free energy landscape (FEL) analysis and binding free energy calculations (MM-PBSA) provided further validation for the promising inhibitory potential of these compounds. The prominent well observed for L1 and L2 in the FEL analysis suggested they form highly stable complexes, with L1 showing particularly strong binding interactions, evidenced by a binding free energy of  $-53.49$  kcal/mol, compared to MEY’s  $-40.74$  kcal/mol. This further substantiates the potential of L1 and L2 as selective and effective HSP90 inhibitors.

Overall, our study demonstrates that *N*-aryl-benzimidazolone analogs L1 and L2 possess excellent binding stability, favorable physicochemical properties, and promising drug-likeness profiles. These compounds (Table 6) could be developed further as potent and selective inhibitors of HSP90, with the potential for therapeutic applications in cancer and other diseases associated with HSP90 dysfunction. Further experimental validation is required to confirm the *in vitro* and *in vivo* efficacy of these compounds, but the findings from our study provide a strong foundation for future drug development efforts targeting HSP90.

**Table 6.** Aryl-benzimidazole derivatives proposed as HSP90 protein inhibitors.

	PubChem CID	Molecular Formula	Structure	IUPAC Name
L1	69438556	C <sub>22</sub> H <sub>20</sub> N <sub>2</sub> O <sub>3</sub>		3-[2,4-dihydroxy-5-(3-phenylpropyl)phenyl]-1H-benzimidazol-2-one
L2	69441313	C <sub>21</sub> H <sub>22</sub> N <sub>2</sub> O <sub>3</sub>		3-[5-[(E)-2-cyclohexylethenyl]-2,4-dihydroxyphenyl]-1H-benzimidazol-2-one



## 5. Conclusions

This study identified *N*-aryl-benzimidazolone analogs as potential inhibitors of the HSP90 protein, a target implicated in various diseases. Using computational methods such as pharmacophore modeling, virtual screening, in silico ADMET prediction, and molecular dynamics simulations, a pharmacophore model based on the target ADDRR was developed based on the ligand MEY. This model screened 30,994 compounds, resulting in the identification of 3019 candidates, of which five compounds showed promising binding affinity ( $-9.795$ ;  $-8.264$  kcal/mol). The top two compounds, L1 and L2, were also found to be stable in molecular dynamics simulations, with favorable parameters such as RMSD, RMSF, Rg, and SASA. These results suggest a potential for the development of effective HSP90 inhibitors, warranting further experimental validation.

**Supplementary Materials:** The following supporting information can be downloaded at: <https://www.mdpi.com/article/10.3390/app142310817/s1>, Table S1: Results of Enrichment Study for Validating the ADDRR Pharmacophore Model; Table S2: The specific type of contact and the amino acid residues involved in that interaction inside the binding pocket of the hsp90 enzyme (3owd) are requested; Table S3: Top Potential Hsp90 Inhibitors Based on Docking Results; Table S4: Medicinal chemistry properties of the top lead compounds; Table S5: In silico prediction of metabolism and excretion of the top lead compounds; Table S6: In silico prediction of toxicity of the top lead compounds. Table S7: Toxicity prediction of the top lead compounds; Figure S1: ROC Plot for Pharmacophore Model Validation of the ADDRR Hypothesis.

**Author Contributions:** R.M., L.B. and A.Z.: Formal analysis, Validation, Data curation, Investigation, Resources, Software, Visualization, Writing—original draft. M.O.: Supervision, Conceptualization, Methodology, Validation. B.Y.A.: Writing—review, editing, funding acquisition. All authors have read and agreed to the published version of the manuscript.

**Funding:** The researchers would like to thank the Deanship of Graduate Studies and Scientific Research at Qassim University for its financial support (QU-APC-2024-9/1).

**Institutional Review Board Statement:** Not applicable.

**Informed Consent Statement:** Not applicable.

**Data Availability Statement:** Data are contained within the article.

**Conflicts of Interest:** The authors declare no conflicts of interest.

## References

1. Bray, F.; Laversanne, M.; Sung, H.; Ferlay, J.; Siegel, R.L.; Soerjomataram, I.; Jemal, A. Global Cancer Statistics 2022: GLOBOCAN Estimates of Incidence and Mortality Worldwide for 36 Cancers in 185 Countries. *CA Cancer J. Clin.* **2024**, *74*, 229–263. [[CrossRef](#)] [[PubMed](#)]
2. Ren, X.; Li, T.; Zhang, W.; Yang, X. Targeting Heat-Shock Protein 90 in Cancer: An Update on Combination Therapy. *Cells* **2022**, *11*, 2556. [[CrossRef](#)] [[PubMed](#)]
3. Birbo, B.; Madu, E.E.; Madu, C.O.; Jain, A.; Lu, Y. Role of HSP90 in Cancer. *Int. J. Mol. Sci.* **2021**, *22*, 10317. [[CrossRef](#)] [[PubMed](#)]
4. Zhang, J.; Li, H.; Liu, Y.; Zhao, K.; Wei, S.; Sugarman, E.T.; Liu, L.; Zhang, G. Targeting HSP90 as a Novel Therapy for Cancer: Mechanistic Insights and Translational Relevance. *Cells* **2022**, *11*, 2778. [[CrossRef](#)]
5. Li, Z.-N.; Luo, Y. HSP90 Inhibitors and Cancer: Prospects for Use in Targeted Therapies (Review). *Oncol. Rep.* **2022**, *49*, 6. [[CrossRef](#)]
6. Xie, X.; Zhang, N.; Li, X.; Huang, H.; Peng, C.; Huang, W.; Foster, L.J.; He, G.; Han, B. Small-Molecule Dual Inhibitors Targeting Heat Shock Protein 90 for Cancer Targeted Therapy. *Bioorganic Chem.* **2023**, *139*, 106721. [[CrossRef](#)]
7. Wright, J.B. The Chemistry of the Benzimidazoles. *Chem. Rev.* **1951**, *48*, 397–541. [[CrossRef](#)]
8. Barker, H.A.; Smyth, R.D.; Weissbach, H.; Toohey, J.L.; Ladd, J.N.; Volcani, B.E. Isolation and Properties of Crystalline Cobamide Coenzymes Containing Benzimidazole or 5,6-Dimethylbenzimidazole. *J. Biol. Chem.* **1960**, *235*, 480–488. [[CrossRef](#)]
9. Preethi, P.; Karthikeyan, E.; Lohita, M.; Teja, P.; Subhash, M.; Shaheena, P.; Prashanth, Y.; Sai, N. Benzimidazole: An Important Scaffold in Drug Discovery. *Asian J. Pharm. Technol.* **2015**, *5*, 138–152. [[CrossRef](#)]
10. Vyas, V.K.; Ghate, M. Substituted Benzimidazole Derivatives as Angiotensin II-AT1 Receptor Antagonist: A Review. *Mini Rev. Med. Chem.* **2010**, *10*, 1366–1384. [[CrossRef](#)]
11. Ardestani, M.; Khorsandi, Z.; Keshavarzipour, F.; Iravani, S.; Sadeghi-Aliabadi, H.; Varma, R.S. Heterocyclic Compounds as Hsp90 Inhibitors: A Perspective on Anticancer Applications. *Pharmaceutics* **2022**, *14*, 2220. [[CrossRef](#)] [[PubMed](#)]

12. Abbasi, M.; Amanlou, M.; Aghaei, M.; Hassanzadeh, F.; Sadeghi-Aliabadi, H. Identification of New Hsp90 Inhibitors: Structure Based Virtual Screening, Molecular Dynamic Simulation, Synthesis and Biological Evaluation. *Anti-Cancer Agents Med. Chem.* **2021**, *21*, 2583–2591. [[CrossRef](#)] [[PubMed](#)]
13. Li, M.; She, X.; Ou, Y.; Liu, J.; Yuan, Z.; Zhao, Q. Design, Synthesis and Biological Evaluation of a New Class of Hsp90 Inhibitors Vibsanin C Derivatives. *Eur. J. Med. Chem.* **2022**, *244*, 114844. [[CrossRef](#)] [[PubMed](#)]
14. Sliwoski, G.; Kothiwale, S.; Meiler, J.; Lowe, E.W. Computational Methods in Drug Discovery. *Pharmacol. Rev.* **2014**, *66*, 334–395. [[CrossRef](#)]
15. Yang, S.-Y. Pharmacophore Modeling and Applications in Drug Discovery: Challenges and Recent Advances. *Drug Discov. Today* **2010**, *15*, 444–450. [[CrossRef](#)]
16. Hollingsworth, S.A.; Dror, R.O. Molecular Dynamics Simulation for All. *Neuron* **2018**, *99*, 1129–1143. [[CrossRef](#)]
17. Bruncko, M.; Tahir, S.K.; Song, X.; Chen, J.; Ding, H.; Huth, J.R.; Jin, S.; Judge, R.A.; Madar, D.J.; Park, C.H.; et al. N-Aryl-Benzimidazolones as Novel Small Molecule HSP90 Inhibitors. *Bioorganic Med. Chem. Lett.* **2010**, *20*, 7503–7506. [[CrossRef](#)]
18. Ouassaf, M.; Belaidi, S.; Mogren Al Mogren, M.; Chtita, S.; Ullah Khan, S.; Thet Htar, T. Combined Docking Methods and Molecular Dynamics to Identify Effective Antiviral 2,5-Diaminobenzophenonederivatives against SARS-CoV-2. *J. King Saud Univ.-Sci.* **2021**, *33*, 101352. [[CrossRef](#)]
19. Ejaz, S.A.; Aziz, M.; Fawzy Ramadan, M.; Fayyaz, A.; Bilal, M.S. Pharmacophore-Based Virtual Screening and In-Silico Explorations of Biomolecules (Curcumin Derivatives) of *Curcuma longa* as Potential Lead Inhibitors of ERBB and VEGFR-2 for the Treatment of Colorectal Cancer. *Molecules* **2023**, *28*, 4044. [[CrossRef](#)]
20. Dong, J.; Wang, N.-N.; Yao, Z.-J.; Zhang, L.; Cheng, Y.; Ouyang, D.; Lu, A.-P.; Cao, D.-S. ADMETlab: A Platform for Systematic ADMET Evaluation Based on a Comprehensively Collected ADMET Database. *J. Cheminform.* **2018**, *10*, 29. [[CrossRef](#)]
21. Banerjee, P.; Eckert, A.O.; Schrey, A.K.; Preissner, R. ProTox-II: A Webserver for the Prediction of Toxicity of Chemicals. *Nucleic Acids Res.* **2018**, *46*, W257–W263. [[CrossRef](#)] [[PubMed](#)]
22. Lotfi, B.; Mebarka, O.; Khan, S.U.; Htar, T.T. Pharmacophore-Based Virtual Screening, Molecular Docking and Molecular Dynamics Studies for the Discovery of Novel Neuraminidase Inhibitors. *J. Biomol. Struct. Dyn.* **2024**, *42*, 5308–5320. [[CrossRef](#)] [[PubMed](#)]
23. Akter, N.; Bourougaa, L.; Ouassaf, M.; Bhowmic, R.C.; Uddin, K.M.; Bhat, A.R.; Ahmed, S.; Kawsar, S.M.A. Molecular Docking, ADME-Tox, DFT and Molecular Dynamics Simulation of Butyroyl Glucopyranoside Derivatives against DNA Gyrase Inhibitors as Antimicrobial Agents. *J. Mol. Struct.* **2024**, *1307*, 137930. [[CrossRef](#)]
24. McDonald, E.; Jones, K.; Brough, P.A.; Drysdale, M.J.; Workman, P. Discovery and Development of Pyrazole-Scaffold Hsp90 Inhibitors. *Curr. Top. Med. Chem.* **2006**, *6*, 1193–1203. [[CrossRef](#)] [[PubMed](#)]
25. Ouassaf, M.; Bourougaa, L.; Al-Mijalli, S.H.; Abdallah, E.M.; Bhat, A.R.; Kawsar, S.M.A. Marine-Derived Compounds as Potential Inhibitors of Hsp90 for Anticancer and Antimicrobial Drug Development: A Comprehensive In Silico Study. *Molecules* **2023**, *28*, 8074. [[CrossRef](#)] [[PubMed](#)]
26. Ouassaf, M.; Daoui, O.; Alam, S.; Elkhatabi, S.; Belaidi, S.; Chtita, S. Pharmacophore-Based Virtual Screening, Molecular Docking, and Molecular Dynamics Studies for the Discovery of Novel FLT3 Inhibitors. *J. Biomol. Struct. Dyn.* **2022**, *41*, 7712–7724. [[CrossRef](#)]
27. Chen, D.; Oezguen, N.; Urvil, P.; Ferguson, C.; Dann, S.M.; Savidge, T.C. Regulation of Protein-Ligand Binding Affinity by Hydrogen Bond Pairing. *Sci. Adv.* **2016**, *2*, e1501240. [[CrossRef](#)]
28. Maowa, J.; Alam, A.; Rana, K.M.; Dey, S.; Hosen, A.; Fujii, Y.; Hasan, I.; Ozeki, Y.; Kawsar, S.M.A. Synthesis, Characterization, Synergistic Antimicrobial Properties and Molecular Docking of Sugar Modified Uridine Derivatives. *Ovidius Univ. Ann. Chem.* **2021**, *32*, 6–21. [[CrossRef](#)]
29. Yasmin, F.; Amin, M.R.; Hosen, M.A.; Bulbul, M.Z.H.; Dey, S.; Kawsar, S.M.A. Monosaccharide derivatives: Synthesis, antimicrobial, pass, antiviral and molecular docking studies against SARS-COV-2 Mpro inhibitors. *Cellulose Chem. Technol.* **2021**, *55*, 477–499. [[CrossRef](#)]
30. Okella, H.; Okello, E.; Mtewa, A.G.; Ikiriza, H.; Kaggwa, B.; Aber, J.; Ndekezi, C.; Nkamwesiga, J.; Ajayi, C.O.; Mugeni, I.M.; et al. ADMET Profiling and Molecular Docking of Potential Antimicrobial Peptides Previously Isolated from African Catfish, *Clarias Gariepinus*. *Front. Mol. Biosci.* **2022**, *9*, 1039286. [[CrossRef](#)]
31. George, O.A. *LipinskiFilters: Computes and Visualize Lipinski's Parameters*, version 1.0.1. 2024.
32. Halford, B. Wrestling with the Rule of 5. *C&EN Global Enterp.* **2023**, *101*, 16–19. [[CrossRef](#)]
33. Young, R.J. Today's Drug Discovery and the Shadow of the Rule of 5. *Expert Opin. Drug Discov.* **2023**, *18*, 965–972. [[CrossRef](#)] [[PubMed](#)]
34. Johnson, T.W.; Dress, K.R.; Edwards, M. Using the Golden Triangle to Optimize Clearance and Oral Absorption. *Bioorganic Med. Chem. Lett.* **2009**, *19*, 5560–5564. [[CrossRef](#)] [[PubMed](#)]
35. Mazri, R.; Ouassaf, M.; Kerassa, A.; Alhatlani, B.Y. Exploring Potential Therapeutics: Targeting Dengue Virus NS5 through Molecular Docking, ADMET Profiling, and DFT Analysis. *Chem. Phys. Impact* **2024**, *8*, 100468. [[CrossRef](#)]
36. Half Life—StatPearls—NCBI Bookshelf. Available online: <https://www.ncbi.nlm.nih.gov/books/NBK554498/> (accessed on 29 October 2024).
37. Amorim, A.M.B.; Piochi, L.F.; Gaspar, A.T.; Preto, A.J.; Rosário-Ferreira, N.; Moreira, I.S. Advancing Drug Safety in Drug Development: Bridging Computational Predictions for Enhanced Toxicity Prediction. *Chem. Res. Toxicol.* **2024**, *37*, 827. [[CrossRef](#)]

38. Swanson, J.M.J.; Henschman, R.H.; McCammon, J.A. Revisiting Free Energy Calculations: A Theoretical Connection to MM/PBSA and Direct Calculation of the Association Free Energy. *Biophys. J.* **2004**, *86*, 67–74. [[CrossRef](#)]
39. Berkmen, Y.M.; Lande, A. Chest Roentgenography as a Window to the Diagnosis of Takayasu's Arteritis. *Am. J. Roentgenol.* **1975**, *125*, 842–846. [[CrossRef](#)]
40. Saxena, S.; Chaudhaery, S.S.; Varshney, K.; Saxena, A.K. Pharmacophore-Based Virtual Screening and Docking Studies on Hsp90 Inhibitors. *SAR QSAR Environ. Res.* **2010**, *21*, 445–462. [[CrossRef](#)] [[PubMed](#)]
41. Sharma, N.; Sharma, M.; Faisal, M.; Alatar, A.A.; Kumar, R.; Ahmad, S.; Akhtar, S. Ligand-Based Pharmacophore Modeling, Molecular Docking and Simulation Studies for the Exploration of Natural Potent Antiangiogenic Inhibitors Targeting Heat Shock Protein 90. *Lett. Drug Des. Discov.* **2023**, *20*, 95–109. [[CrossRef](#)]
42. Arnott, J.A.; Planey, S.L. The Influence of Lipophilicity in Drug Discovery and Design. *Expert Opin. Drug Discov.* **2012**, *7*, 863–875. [[CrossRef](#)]
43. Fusani, L.; Palmer, D.S.; Somers, D.O.; Wall, I.D. Exploring Ligand Stability in Protein Crystal Structures Using Binding Pose Metadynamics. *J. Chem. Inf. Model.* **2020**, *60*, 1528. [[CrossRef](#)] [[PubMed](#)]

**Disclaimer/Publisher's Note:** The statements, opinions and data contained in all publications are solely those of the individual author(s) and contributor(s) and not of MDPI and/or the editor(s). MDPI and/or the editor(s) disclaim responsibility for any injury to people or property resulting from any ideas, methods, instructions or products referred to in the content.